Lateral Spreading within a Limit Equilibrium Framework: Newmark Sliding Blocks with Degrading Yield Accelerations

Ben A. Leshchinsky[1], H. Benjamin Mason[2], Michael J. Olsen[3], Daniel T. Gillins[4]

[1]Assistant Professor, Department of Forest Engineering, Resources and Management & School of Civil and Construction Engineering Oregon State University, 273 Peavy Hall, Corvallis, OR 97331, Phone:+1-541-737-8873, Email: ben.leshchinsky@oregonstate.edu
[2]Associate Professor, School of Civil and Construction Engineering Oregon State University, 213 Owen Hall, Corvallis, OR 97331, ben.mason@oregonstate.edu
[3]Associate Professor, School of Civil and Construction Engineering Oregon State University, 311 Owen Hall, Corvallis, OR 97331, michael.olsen@oregonstate.edu
[4]Geodesist, NOAA/National Geodetic Survey (N/NGS4), 1315 East-West Highway, SSMC3, Silver Spring, MD 20910, former assistant professor at Oregon State University,, daniel.gillins@noaa.gov

ABSTRACT

Lateral spreading is a prevalent geotechnical problem associated with earthquake-induced liquefaction, often occurring at gentle slopes of loose, saturated sand near bodies of water and causing significant damage to buried utilities. This study presents a deterministic approach to analyze lateral spreading behavior using a modified Newmark analysis applied to a column of sliding blocks with degrading yield accelerations. The proposed sliding column approach exhibits reasonable agreement with a well-instrumented, centrifuge test evaluating free-field lateral spreading. The analysis captures lateral spreading displacement throughout a soil profile as well as shear strains and simplified earth pressures. The effect of light cementation is investigated, demonstrating notable arrest of lateral spreading displacements and pressures. Free face effects are also evaluated for a liquefying layer of soil beneath a gentle, competent crustal slope, demonstrating notable lateral spreading behavior with larger inclinations of liquefying soil. However, lateral spreading still occurred when considering a horizontal liquefying layer, realized due to inertial loading and differences between confining boundary forces. The

approach can be utilized to efficiently analyze lateral spreading across a large spatial extent.

Keywords: Limit Equilibrium, Lateral Spreading, Liquefaction, Earthquakes, Natural Hazards

INTRODUCTION

Lateral spreading is generally considered the most pervasive type of liquefaction-induced ground failure generated by earthquakes (NRC 1985). When lateral spreading occurs, mostly intact blocks of surficial, crustal soil situated atop weak, liquefied strata displace down gentle slopes. Lateral spreading often occurs towards areas of large topographic relief (e.g. river channels, marine structures). The laterally-spreading blocks may encompass large areas, displacing several meters and generating large lateral loads on buried structures, resulting in considerable damage to bridges, buildings, pipelines, roadways, marine structures and more. Assessing lateral spreading potential and displacements has primarily been performed using case history-based statistical methods, experimental approaches and analytical approximations using Newmark sliding block analyses.

A promising means of evaluating lateral spreading, while incorporating aspects of topography, soil conditions and porewater pressures, is the use of a limit equilibrium analysis that accounts for time-dependent excess porewater pressure (PWP) buildup and inertial loading for a series of sliding blocks. These analyses frequently implement rigid body mechanics (e.g. a "rigid" sliding block) considering limit state equilibrium with a sum of forces, moments or both. Unfortunately, the typical rigid body assumption is a limitation when considering liquefying sandy soil, which has a relatively low volumetric threshold strain between elastic and plastic response (i.e., approximately 0.01 to 0.02%; Vucetic 1994). Limit equilibrium approaches are also hindered by an inability to determine displacements; i.e., limit equilibrium analyses implicitly only capture the ultimate limit state, which is representative of complete collapse and instability, and neglects displacements at failure. Fortunately, the modified Newmark approach (Newmark 1965) merges the simplicity of limit equilibrium analyses with displacement estimation via a determined yield acceleration, k_y, for a given sliding block. Note that k_y is the horizontal pseudostatic seismic coefficient, k_h, that causes limit equilibrium failure for a given sliding block. To determine global displacement of a sliding block with the modified Newmark method, the earthquake motion acceleration values that exceed the yield acceleration are double-integrated as a function of time.

A potential means for capturing the time-dependent interaction of excess porewater pressure with inertial loading in a limit equilibrium analysis is the consideration of time-dependent yield accelerations. A buildup of excess porewater pressure reduces the frictional shear strength of a given soil, ultimately lowering the yield acceleration required for permanent displacement to occur. Matasovic and Kavazanjian (1997) evaluated Newmark displacements considering degrading yield accelerations. Biondi et al. (2000) extended this approach to an infinite slope analysis for coarse-grained, saturated soil, further compounding the effects of excess porewater pressures on slope stability and realized displacements. Kramer and Smith (1997) expanded upon the concept of a singular sliding block for slope stability analyses by considering a series of coupled sliding blocks with dashpots to evaluate displacements above a given sliding plane. The Kramer and Smith (1997) method is particularly useful for large landfill slopes that are characterized by low natural frequencies.

The present study extends the previous research to a column of sliding blocks, which is used in a limit equilibrium/modified Newmark framework to evaluate displacement profiles, shear strains, liquefaction depth and earth pressures. The primary goal of the article is presenting the mechanics used to develop the modified Newmark framework for predicting liquefaction-induced lateral spreading displacements (i.e., the methodology). In addition, a simple verification exercise is performed using results from a well-documented centrifuge test (Sharp and Dobry 2002) and some preliminary results are discussed.

BACKGROUND

Due to the complexity associated with observed post-earthquake lateral spreading, displacement models are mostly limited to statistical regression analyses of well-documented case histories (Bartlett and Youd 1995, Rach and Martin 2000, Youd et al. 2002, Zhang et al. 2004, Gillins and Bartlett 2013). Regression models used to estimate lateral spreading-based displacements are often based on topographic, geotechnical, and seismic data. Important input parameters used with empirical and semi-empirical models for estimating lateral spread displacements include: free-face ratio, ground slope, standard penetration test (SPT) blow counts ($N_{1,60}$), mean grain size (D_{50}), fines content (F), earthquake magnitude (M), and distance to the seismic source (R), within liquefiable layers (Youd et al. 2002, Bartlett and Youd 1995, Gillins and Bartlett 2013). The most widely used technique in practice is the Youd et al. (2002) empirical procedure (Olson and Johnson, 2008), which was developed by multilinear regression (MLR) of a large case history database. Using the same case history database, Gillins and Bartlett (2013) revised the MLR empirical procedure to use more widely available geotechnical data, thereby making the procedure more implementable for regional mapping of lateral spread hazards. Following the work of Gillins and Bartlett (2013) and Franke and Kramer (2014), Ekstrom and Franke (2016) used the empirical lateral spread displacement database to develop a simplified performance-based prediction methodology, which is also applicable to regional-scale hazard mapping. Such maps are useful for conveying hazards to public utility companies, risk managers, and the earthquake engineering community. Nonetheless, there is still limited susceptibility and hazard mapping of liquefaction-induced lateral spread based on generalized, mechanistic analyses.

Within regions susceptible to liquefaction, it is critical to evaluate potential displacements and structural loads induced by the temporary soil instability. Displacements due to lateral spread have been evaluated using a variety of methods, particularly using a modified Newmark (1965) analysis, which is an accepted practical approach to estimating displacements of slopes (Wartman et al. 2003, Kramer and Smith 1997), walls (Rathje and Bray 2000, Matasovic and Kavazanjian 1997, Whitman and Liao 1985) and other structures under seismic loading. Olson and Johnson (2008) found that classical Newmark-based back-calculations coincided well with lateral spreads from various well-documented case studies and suggested that cone penetration tests (CPT) were particularly useful for determining liquefaction potential. Brandenberg et al. (2007) used a sliding block and wedge failure method to evaluate the moment and shear profiles on a series of piles underneath a pile cap subject to lateral spreading. Notably, the cap was treated as a sliding block subject to inertial loading, and Brandenberg et al. (2007) corroborated analytical models with centrifuge testing. Taboada and Dobry (1998) used centrifuge testing to evaluate lateral spreads for various slopes and configurations, and found that dilation during lateral spreading possibly reduces excess porewater pressures during shear; thus, potentially arresting the lateral spreads. Similar approaches for non-linear resistance of sliding blocks have been implemented for other sliding block analyses (e.g. Rathje and Bray 2000). However, these approaches have generally been related to centrifuge tests or case studies, which are limited in application for evaluating regions of lateral spread. Despite the prevalence of lateral spreading of gentle slopes and slopes near free face relief, research evaluating lateral spreading as a generalized slope stability problem is scarce. Development of a limit equilibrium analytical framework for evaluating lateral spread-induced displacements and loading as a time-dependent problem enables hazard assessment based on principles of soil mechanics, which broadens the applicability of the methods and enhances existing geotechnical design approaches.

The proposed limit equilibrium approach evaluates yield accelerations of multiple thin, rigid slices within a soil column. The time-dependent yield accelerations are determined throughout the soil column, and ultimately, the displacement for each discretized slice for a given acceleration-time series is determined. The proposed limit equilibrium approach assumes liquefying soil is a viscous material that does not fail as a rigid element. By evaluating numerous thin slices placed in a column of sliding blocks and solving for boundary forces on each slice, the liquefiable layer is “laminar,” which enables the evaluation of equilibrium within each thin sliding element (i.e., effectively discretizing the liquefying soil). Furthermore, evaluation of boundary forces (e.g., slice weights, lateral earth pressure resultants, shear resistance, pseudo-static seismic acceleration) and boundary neutral forces (e.g., porewater pressure, excess porewater pressures) surrounding each slice enables a time-dependent analysis of displacements under seismic acceleration as well as the determination of a time-dependent yield acceleration that accounts for the deleterious effects of excess porewater pressure buildup. That is, the column of slices representative of liquefiable soil are evaluated in a limit equilibrium framework for specified time increments using a modified Newmark approach for sliding blocks with changing yield accelerations from excess porewater pressure buildup. Thus, it captures not only the laminar, "flexible" displacements throughout the depth of a liquefying, lateral spreading layer, but related earth pressures, depth of liquefaction front (i.e. where the lateral spreading has initiated), and shear strain throughout a given soil profile. The analyses performed herein often overestimates lateral spreading displacements due to omission of complex behavior (e.g., dilative and viscous behavior of liquefied soil); nevertheless, the analysis framework presents a useful deterministic means of evaluating lateral spreading and related trends.

METHODOLOGY

The proposed framework evaluates lateral spreading using a limit equilibrium analysis similar to that presented by Biondi et al. (2000), but applied to a column of Newmark sliding blocks with time-dependent shear strength (dependent on input excess pore water pressures) and time-dependent driving forces (seismic acceleration). The column of sliding blocks (Figure 1) is analyzed with the modified Newmark approach with time-dependent yield accelerations subject to excess pore water pressures and seismic motions. Cumulative displacements of both crustal layers and liquefying soil is subsequently used to generate (1) displacement profiles, (2) shear strain profiles, (3) liquefied earth pressures, and (4) liquefaction front depths. The results demonstrate good agreement with well-instrumented centrifuge tests investigating lateral spreading for soil having a small inclination (~5°) with buildup of excess porewater pressure and seismic excitation (Sharp and Dobry 2002).

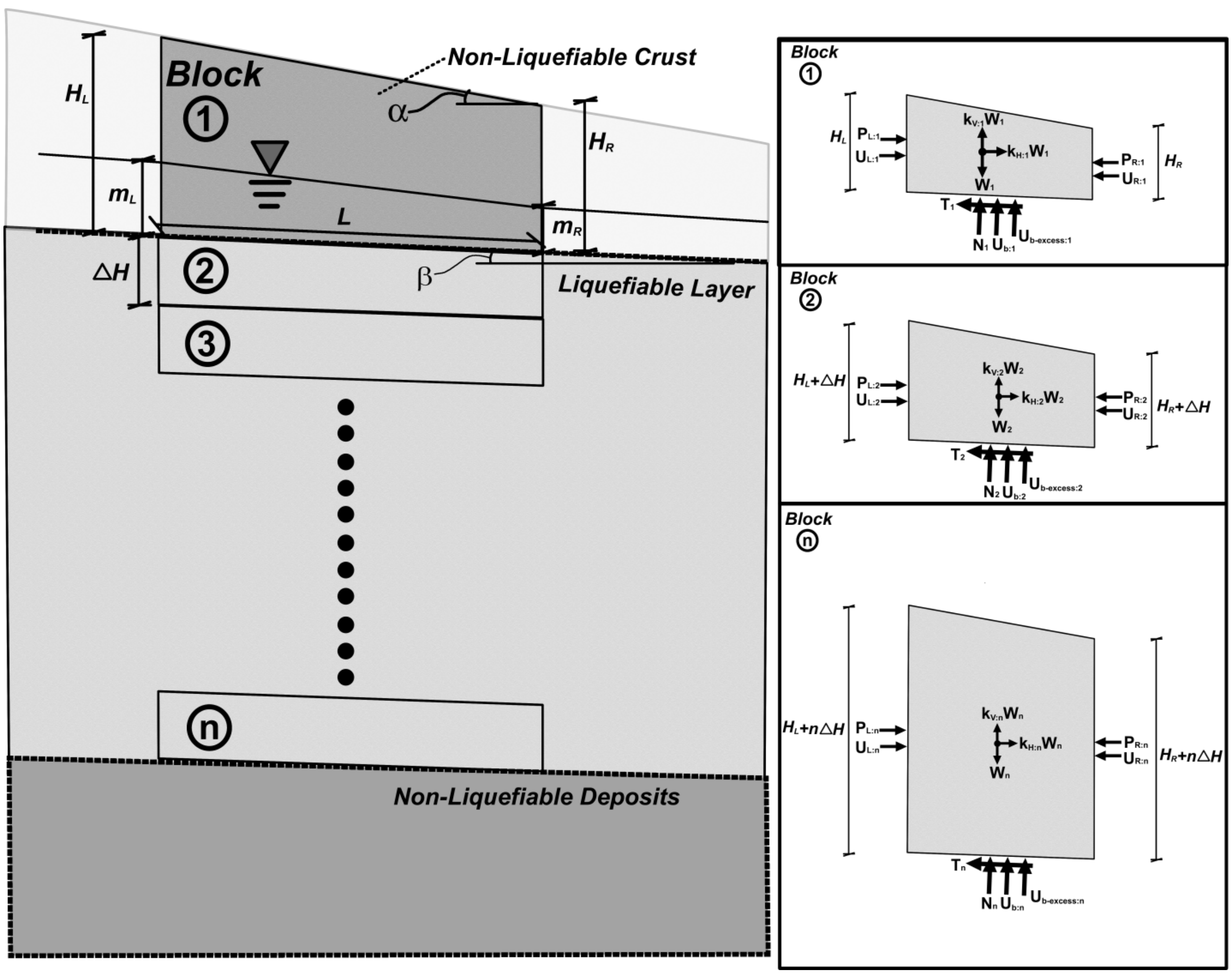

Figure 1. Free-body diagrams of sliding blocks under liquefaction conditions.

As previously mentioned, lateral spreading occurs when relatively intact blocks of soil slide as excess porewater pressures increase in subsurface layers, which reduces the shear strength and can lead to liquefaction. These preceding conditions can be modeled by a simplified sliding block analysis (Figure 1) defined by a trapezoidal block with boundary depths, H_L and H_R, a surface slope, α, above a layer of liquefiable soil with slope angle, β, and length, L. The weight of the block is W, the inertial forces are $k_v W$ and $k_h W$, the normal resultant force is N, the shear resistance force is T, the boundary earth pressure resultants are P_L and P_R, the lateral boundary hydraulic resultant forces are U_1 and U_2, the base boundary hydraulic resultant force representative of a static phreatic surface is U_b, and an excess pore water pressure resultant force that may induce lateral spread is $U_{b-excess}$. These porewater pressures are not explicitly determined in the presented framework, but can be determined from experimental results, numerical models, site response analyses, or simplified theoretical approaches such as Seed et al. (1977). A series of n sliding blocks can be represented similarly by adding perpendicular forces on top of a block, which represents the overburden of both the intact surficial block and the liquefied soil above.

Considering pseudostatic forces perpendicular and parallel to the basal, liquefied slip surface, static equilibrium can be determined for each slice as:

$$\sum F_{\parallel} = 0 = (P_{L:n} + U_{L:n})cos\beta - k_{v:n}W_n sin\beta + k_{h:n}W_n cos\beta + W_n sin\beta - (P_{R:n} + U_{R:n})cos\beta - T_n \quad (1)$$

$$\sum F_{\perp} = 0 = N_n + U_{b:n} + U_{b:n-excess} + (P_{L:n} + U_{L:n})sin\beta + k_{v:n}W_n cos\beta + k_{h:n}W_n sin\beta - W_n cos\beta - (P_{R:n} + U_{R:n})sin\beta \qquad (2)$$

where W_1 is the weight of the crustal block and W_n is the summed weight of laminar slices, which are both defined for a unit depth (i.e., for a 2D problem) as:

$$W_n = W_1 + \sum_{2}^{n} [0.5\gamma_n L(H_{L:n} + H_{R:n} - m_{L:n} - m_{R:n})(1) + 0.5\gamma_{sat:n} L(m_{L:n} + m_{R:n})(1)]$$

(3)

Herein, for simplicity, a linear phreatic surface is assumed where the basal hydrostatic pore pressure resultant, $U_{b:n}$, is defined as:

$$U_{b:n} = U_{b:1} + \sum_{2}^{n} 0.5\gamma_w L(m_{L:n} + m_{R:n})(1) \qquad (4)$$

The shear force resultant is:

$$T_n = \tau_n L \qquad (5)$$

Substituting (5) into (1), static equilibrium parallel to the basal liquefying surface can be determined as:

$$\sum F_{\parallel} = 0 = (P_{L:n} + U_{L:n})cos\beta - k_{V:n}W_n sin\beta + k_{H:n}W_n cos\beta + W_n sin\beta - (P_{R:n} + U_{R:n})cos\beta - \tau_n L \qquad (6)$$

where mobilized shear stress is defined as:

$$\tau_{n-mob} = \frac{c_n{}' + \sigma_n' \sigma_n{}' tan\phi_n'}{FS} \qquad (7)$$

Assuming a length, L, the mobilized shear force resistance becomes:

$$T_{n-mob} = \tau_{n-mob}L = \frac{c_n{}'L + \sigma_n{}'Ltan\phi_n'}{FS} \qquad (8)$$

Because the normal force, N_n, is equal to $\sigma' L$, equation 8 can be rewritten as:

$$T_{n-mob} = \tau_{n-mob}L = \frac{c_n{}'L + N_n\, tan\phi_n'}{FS} \quad (9)$$

Substituting mobilized shear strength (Equation 9) into equation (6) yields:

$$\sum F_{\parallel} = 0 = (P_{L:n} + U_{L:n})cos\beta - k_{v:n}W_n sin\beta + k_{h:n}W_n cos\beta + W_n sin\beta - (P_{R:n} + U_{R:n})cos\beta - \frac{c_n{}'L + N_n\, tan\phi_n'}{FS} \quad (10)$$

By substitution, solving for N_n from equation (2) results in:

$$N_n = W_n cos\beta + (P_{R:n} + U_{R:n})sin\beta - U_{b:n} - U_{b:n-excess} - (P_{L:n} + U_{L:n})sin\beta - k_{v:n} W_n cos\beta - k_{h:n} W_n sin\beta \quad (11)$$

Substituting N_n into equation (10) and solving for the factor of safety (FS) yields:

$$FS = \frac{c_n{}' L + [W_n cos\beta + (P_{R:n} + U_{R:n})sin\beta - U_{b:n} - U_{b:n-excess} - (P_{L:n} + U_{L:n})sin\beta - k_{v:n} W_n cos\beta - k_{h:n} W_n sin\beta] \tan\phi'_n}{(P_{L:n} + U_{L:n})cos\beta - k_{v:n} W_n sin\beta + k_{h:n} W_n cos\beta + W_n sin\beta - (P_{R:n} + U_{R:n})cos\beta} \quad (12)$$

The FS represents the sliding stability of a given block under given seismic and hydraulic conditions. The FS can be evaluated with a time series of excess pore water pressures (u_{excess}) at the base, which may increase due to the seismic accelerations (i.e., liquefaction). A given excess pore water pressure profile is defined as an increase above hydrostatic water pressures, because pressurized water cannot dissipate rapidly during strong shaking. Ultimately, the excess PWP buildup affects the sliding resistance of the block by increasing its "buoyancy." The excess PWP resultant force for a unit width is:

$$U_{b:n-excess}(t) = (u_{n:excess}(t))(L)(1) \quad (13)$$

The effective stress conditions can be defined by an excess porewater pressure coefficient, r_u, which is commonly used to quantify the onset of liquefaction. For this analysis, r_u is defined as:

$$r_u = \frac{u_{excess}}{\sigma_{eff}} = \frac{U_{b:n-excess}}{W_n cos\,(\beta) - U_{b:n}} \quad (14)$$

The excess PWP for a given time increment can be computed and used in the FS equation (Figure 2b). Note that the excess PWP reduces the stability of the sliding block, possibly to the point of sliding (i.e., FS = 1). When FS = 1, the yield acceleration, $k_{H:n\text{-}yield}$, can be defined as:

$$k_{H:n-yield}(t) = \frac{c_n{}'L + [W_n cos\beta + (P_{R:n} + U_{R:n}) sin\beta - U_{b:n} - U_{b:n-excess}(t) - (P_{L:n} + U_{L:n}) sin\beta] \tan\phi_n' - (P_{L:n} + U_{L:n}) cos\beta + (P_{R:n} + U_{R:n}) cos\beta - W_n sin\beta}{(W_n sin\beta \tan\phi_n' + W_n cos\beta)}$$

(15)

which is a function of time and depth. For each thin slice, a Newmark sliding block analysis can then be performed for given time-dependent yield accelerations. This is performed by quantifying the relative acceleration at a given depth at a specific time, which is evaluated as the difference between a given time-dependent yield acceleration ($k_{h:n\text{-}yield}$) and a recorded acceleration ($k_{h:n\text{-}input}$); that is:

$$k_{H:rel}(t) = k_{H:n-input}(t) - k_{H:n-yield}(t)$$

The relative acceleration, k_{rel}, can then be integrated once to determine slice relative velocity, v_{rel}, defined as:

$$v_{rel}(t) = v_{rel}(t_o + \Delta t) + \int_{t_o+\Delta t}^{t} k_{H:rel}(t)\, dt$$

and then integrated a second time to determine the slice relative displacement, d_{rel}, defined as:

$$d_{rel}(t) = \int_{t_o+\Delta t}^{t} v_{rel}(t)\, dt$$

The displacements of each thin slice can then be integrated from the base of the liquefying layer to a depth of concern to evaluate a cumulative displacement profile along a given soil column (Figure 2), defined as:

$$d(t) = \int_{H+n\Delta H}^{H} d_{rel}(t)\, dH$$

In addition, the resultant of downslope liquefied earth pressures for each slice (P_R) can be determined, which gives an estimate of the potential lateral loads on structural elements subjected to lateral spreading (e.g., bridge piers, retaining walls, marine structures). Furthermore, the acceleration-time series of aftershocks can be considered, which enables the estimation of lateral spreading caused after the mainshock.

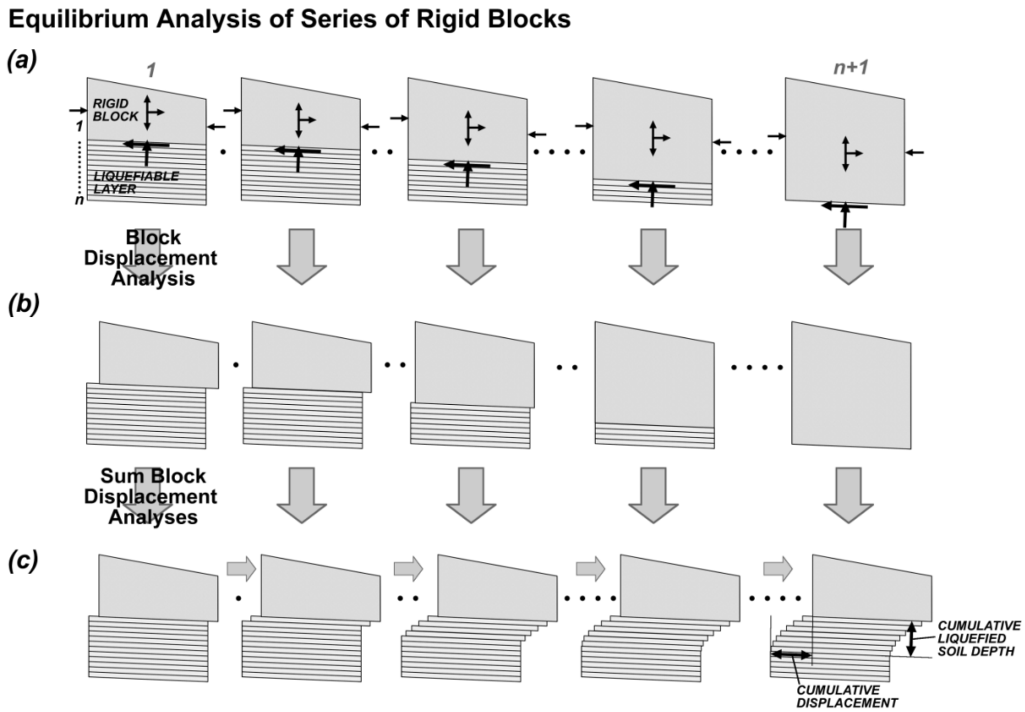

Figure 2. Sliding block series used to estimate earth pressures or cumulative displacements.

MODEL VERIFICATION: COMPARISON TO EXPERIMENTAL DATA

To evaluate the sliding block model, a comparison with results from experimental testing was performed. Contrary to the complexity and uncertainties associated with lateral spreading in post-earthquake assessments, significant experimentation has been performed under controlled conditions to isolate and study the mechanics of lateral spreading. Notably, various researchers have used geotechnical centrifuge testing to investigate lateral spreading, which is often evaluated for structural systems such as bridge foundations (e.g., Abdoun and Dobry 2002, Abdoun et al. 2003, Brandenberg et al. 2005, Brandenberg et al. 2007). To isolate free-field conditions, a well-instrumented experimental series evaluating lateral spreading within a centrifuge was also performed

(Sharp and Dobry 2002) within a laminar box of saturated Nevada sand excited with an input seismic motion. Although the experimental results from several tests are presented, the most comprehensive measurements were presented for model L45V-2-10, consisting of cohesionless Nevada Sand at a 45% relative density (e_{min}=0.516, e_{max}=0.894 corresponding to $\gamma_{dry-max}$=17.33 kN/m^3 and $\gamma_{dry-min}$=13.87 kN/m^3, respectively) with a saturated unit weight of γ_{sat}=19.4 kN/m^3 and effective friction angle of ϕ'=35° (Arulmoli et al. 1992, Mikola and Sitar 2013). The L45V-2-10 model was 0.2 meters (model scale) in height and experienced a centrifugal acceleration of 50 g (prototype height =10 meters), as shown in Figure 3. The L45V-2-10 model, inclined at β=2°, is scaled to a prototype inclination of β=5° under centrifugal conditions when correcting for the weight of the laminar rings and hydrostatic conditions (Taboada 1995, Sharp and Dobry 2002, Sharp et al. 2003). During the test, excess porewater pressures were recorded at prototype depths of 1.25, 2.5, 5.0 and 7.5 meters (Figure 4). Similarly, accelerations from a given input motion (a_{max}=0.2g, f=2 Hz, 22 sinusoidal loading cycles) were recorded at depths of 0.5, 2.5, 5.0 and 7.5 meters (Figure 4). Lateral displacements were recorded at the surface and prototype profile depths of 1.25, 2.5, 6.25 and 7.5 meters. This test, although relatively simple, consisting of homogenous material, was selected for its well-monitored response and well-characterized geotechnical conditions.

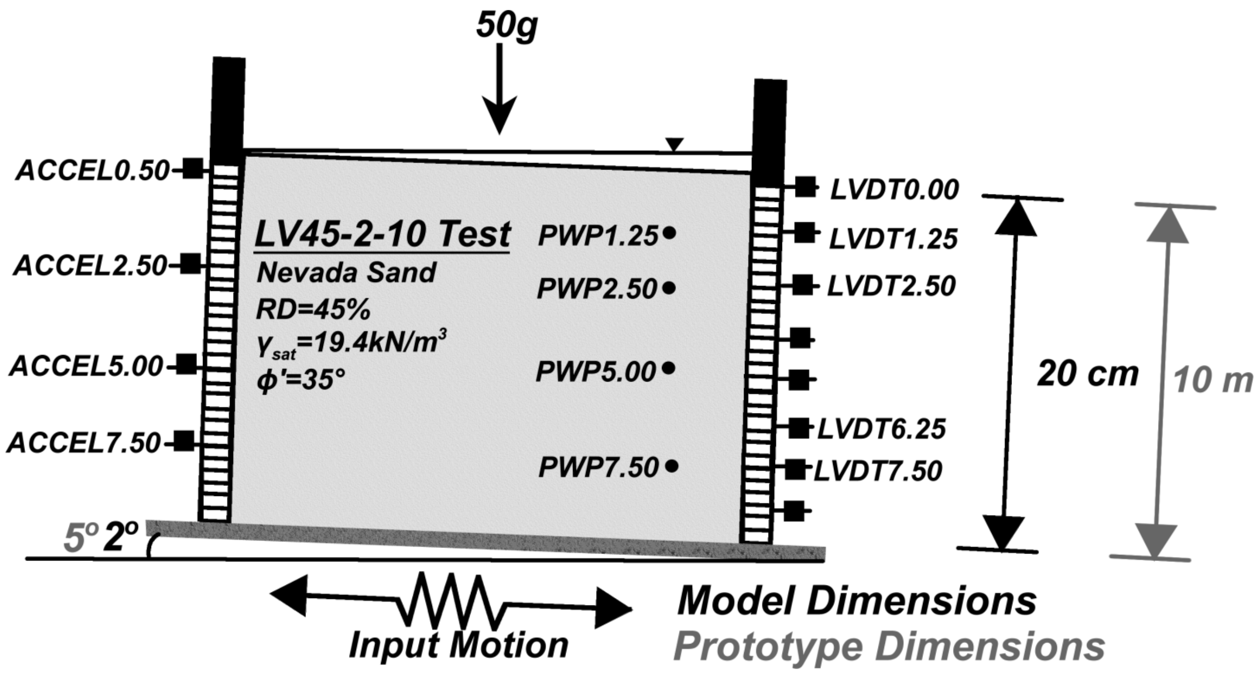

Figure 3. Schematic of LV45-2-10 centrifuge test and instrumentation (after Sharpt and Dobry, 2002).

The Newmark sliding column model was evaluated using the soil conditions and prototype geometry of test L45V-2-10 with the measured excess porewater pressure and acceleration-time series as inputs. The analysis was coded within a MATLAB script that implemented the equations presented within the methodology section with the inputs from the experiment presented by Smith and Dobry (2002). The presented experimental data was recorded at discrete depths in the soil profile; accordingly, linear interpolation was performed between measured excess pore water pressures for the profile at given time increments (Δt=0.1 second), constrained to zero at the surface and kept constant from depths of 7.5 meters to 10 meters. The latter assumption is reasonable, because Sharp and Dobry (2002) report r_u values of less than 70% at depths greater than 7.5 meters in later stages of testing, which are agreeable with values computed by the sliding column model. The acceleration-time series were treated similarly; that is, they were linearly interpolated between recorded depths at a specific time increment with the exception that the input motion was used at the full depth (i.e., 10 meters). The soil column was discretized into 100 increments; i.e., each increment is 0.1 meters in depth. The analysis did not demonstrate significant sensitivity after approximately 100 increments in depth. The surficial soil block was neglected as the experiment was performed on saturated sand with no coherent, crustal block.

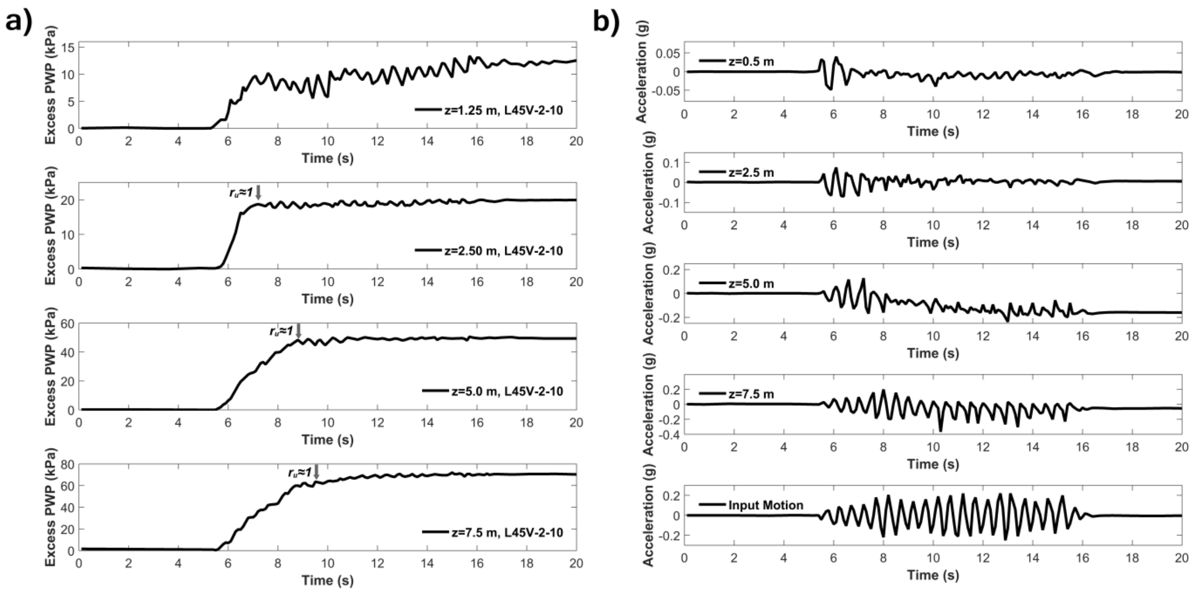

Figure 4. Recorded (a) excess porewater pressure and (b) acceleration data at scaled prototype depths for centrifuge test L45V-2-10 (Taboada and Dobry 1998, Sharp and Dobry 2002).

Comparison of the Newmark sliding column analysis with the experimental results for model L45V-2-10 from Sharp and Dobry (2002) demonstrate reasonable agreement, particularly for determining the initiation time and depth of lateral spreading. For example, Figure 4 shows the depth of the liquefaction front versus the depth where displacement is occurring, and reasonable agreement between the model and the experiment can be observed. More specifically, Figure 5 exhibits a relatively rapid transition towards a liquefied state from the surface to the basal layer between times of 6.5 and 8 seconds. Figure 5 shows that the aforementioned transition is observed in the displacement profiles of the experimental layer as well, where lateral spreading initiates in the upper portion of the soil, transitioning to increasing depths with additional loading cycles. The agreement is notable for approximately the first eight seconds of shaking, but diverges for the final three seconds as the Newmark analysis becomes unstable. For the upper regions of the soil profile, small confining pressures and high porewater pressures result in excessive model displacements after approximately 13 seconds, while the experimental prototype demonstrated arrested movements after shaking. The model overprediction is more muted at greater depths, exhibiting a similar arrest of displacement after shaking cessation. Some of the disagreement between the modeled and experimental results is likely caused by uncertainties in excess porewater pressures and accelerations between transducers as well as the omission of complex parameters that may be associated with liquefied soil, such as viscous and dilative behavior of the saturated sand. Furthermore, the presented analysis does demonstrate a well-known limitation of Newmark displacement analyses – a propensity to exhibit excessively large (and conservative) displacements when notable difference exists between the yield and input accelerations (Jibson 2011), as shown in Figure 6. Despite these drawbacks, the presented sliding column analysis demonstrates a reasonable and simple deterministic means of evaluating lateral spreading displacements in consideration of excess porewater pressures and seismic accelerations, especially during the initial onset of lateral spreading.

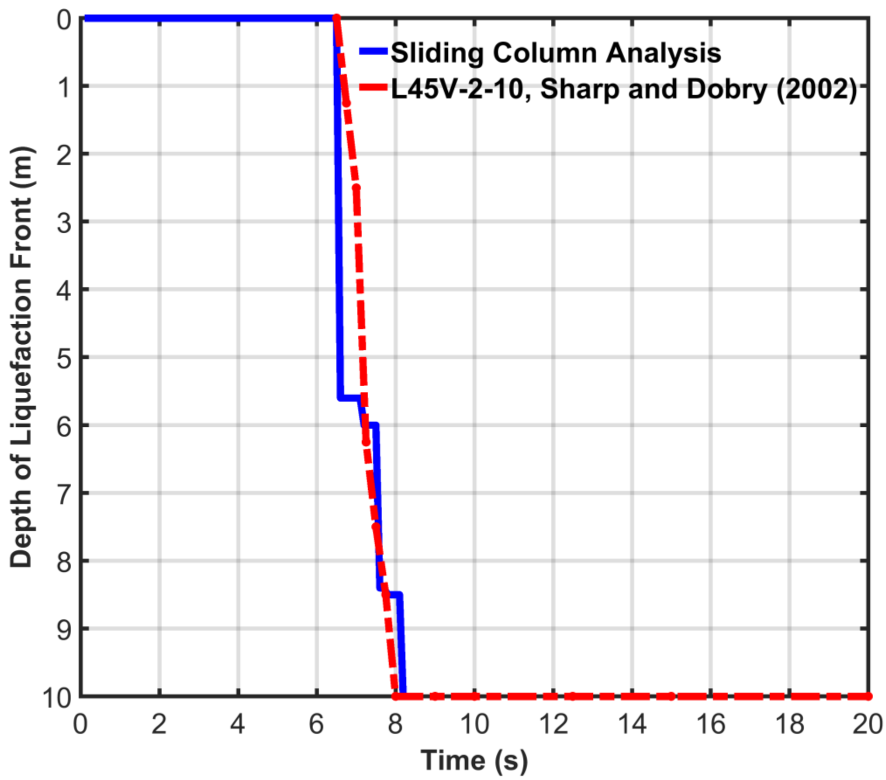

Figure 5. Depth of liquefaction front from centrifuge experiment L45V-2-10 (Sharp and Dobry, 2002) and sliding column analysis.

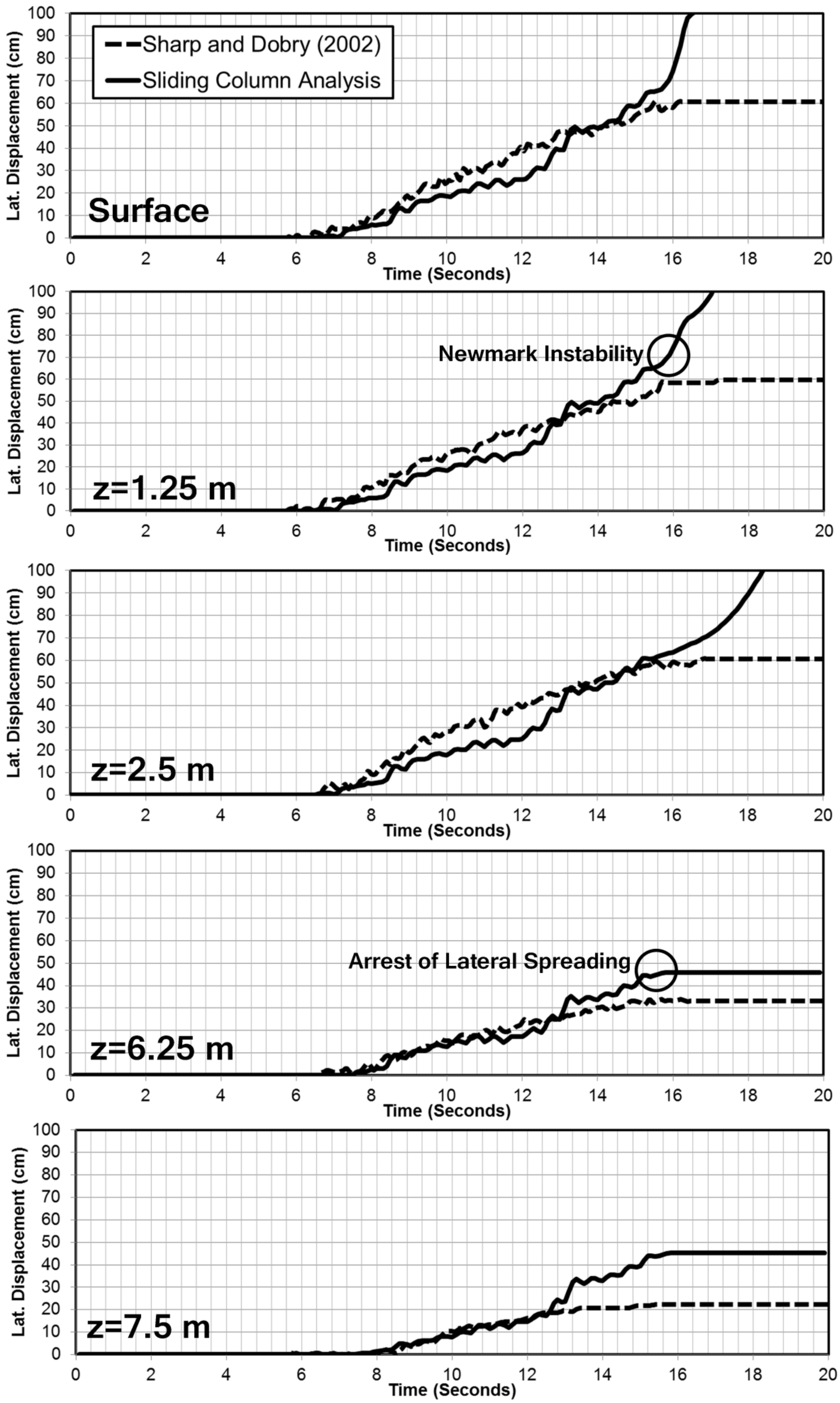

Sharp and Dobry (2002)
Sliding Column Analysis
Surface
Newmark Instability
z=1.25 m
z=2.5 m
Arrest of Lateral Spreading
z=6.25 m
z=7.5 m
Lat. Displacement (cm)
Time (Seconds)

Figure 6. Recorded movement from both experiment (Sharp and Dobry, 2002) and proposed sliding block analysis.

DISCUSSION

The presented sliding column analysis demonstrates a means of evaluating lateral spreading displacements under a variety of scenarios. Furthermore, it enables assessment of various behaviors associated with lateral spreading other than lateral displacement, including assessment of earth pressures and shear strain – parameters that have notable implications on buried structures, such as sewers, pipelines, foundations and marine shoring. The effects of soil unit weight, cementation, liquefying layer slope and free face topography are investigated using the baseline prototype geometry used for test LV45-2-10 (Sharp and Dobry 2002).

Earth Pressures and Shear Strains

A benefit of the proposed sliding column analysis is the direct assessment of earth pressures and shear strains within a 10 meter-deep soil profile for test LV45-2-10. Shear strains can be calculated by dividing the displacement increment for a given slice by the slice depth. The calculated shear strain profile (Figure 7), highlights the notable planes of liquefaction-induced failure. In the case of the LV45-2-10 model, the primary plane of failure occurred at approximately 2.5 meters in depth with other notable planes occurring 7.5 and 9.5 meters in prototype depth. The peaks in shear strain correspond to inflections in the displacement profile (Figure 7). Practically, shear strain and displacement profiles are important for assessing the effects of lateral spreading on buried, linear utilities (e.g. sewers, cables) that cannot withstand significant deformation, particularly differential displacements. Earth pressures can be determined by setting the factor of safety, FS, in equation (12) to unity and solving for P_2, which is in turn discretized into pressure by dividing the resisting force by a given depth increment. The simplification required to calculate earth pressures does not account for seismic boundary forces, but may be considered reasonable for a one-dimensional sliding column with equivalent left and right boundaries. The earth pressures calculated with the sliding column model tend to peak within regions of significant shear strains and displacements, because each sliding block is inherently unstable and exhibits larger earth pressures on its downslope end. This peaking effect is demonstrated at the base by a transition from initial earth pressures to increased pressures - 80 kPa to 95 kPa - between 10 and 14 seconds of testing, respectively. The demonstrated pressure distribution is representative of a mass of soil moving along the liquefying plane, not accounting for localized, wedge-type earth pressures (e.g. Brandenberg et al. 2007) that may impart different loading phenomena.

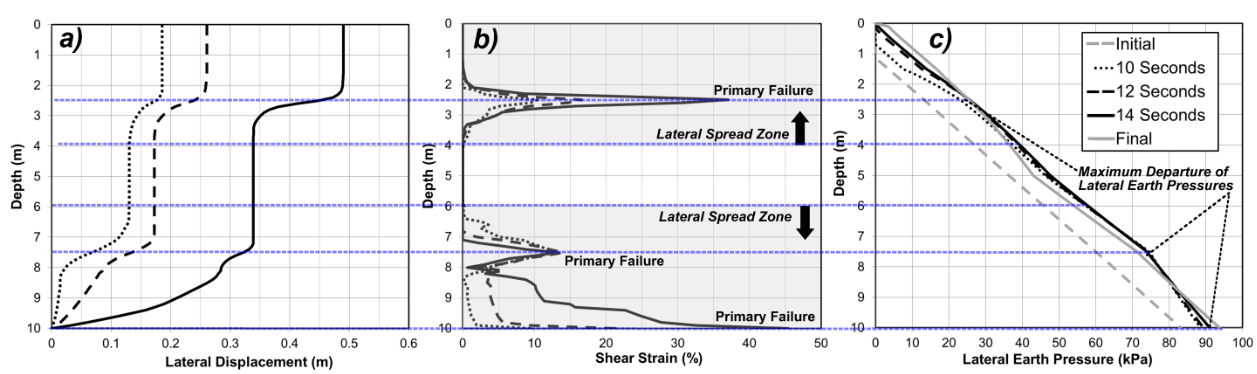

Figure 7. (a) Displacement profiles. (b) Associated shear strains for modeled lateral spread. (c) Associated lateral earth pressures for modeled lateral spread.

Impact and Sensitivity of Pore Water Pressures

The phenomenon of liquefaction and associated lateral spreading is dependent on the generation of excess porewater pressures and effective stress, the latter of which incorporates the unit weight of a soil. When the effective stress of a given soil approaches zero (e.g. r_u=1), the mobilized frictional strength is neutralized, which can result in weakened foundations, excessive displacement of buried utilities, and lateral spreading, among other phenomena. To demonstrate the impacts of varying excess pore water pressure ratios and the associated sensitivity of the sliding column model, an analysis was performed using the same inputs for LV45-2-10, but reducing the maximum r_u values recorded in the testing to 80% and 90% of observed levels. The results (Figure 8) exhibit rapid and excessive lateral spreading when only 100% of observed r_u are used, demonstrated by a steep displacement curve occurring between 16 and 18 seconds. It is noted that the frictional and resisting effects of the laminar rings in the centrifuge testing apparatus may restrict some of the large displacements; however, this observed behavior is still likely an artifact of Newmark-type analyses. Use of 90% and 80% of observed r_u values present a generally inverse trend; that is, lateral spreading displacements are muted at all depths, limiting most of the observed displacements to beyond 7.5 meters in depth. When excess porewater pressure ratios are smaller, the liquefaction front progresses slightly less rapidly – taking two to three more loading cycles to produce lateral spreading displacement at all depths (Figure 9). The preceding analysis demonstrates that the sliding column model is inherently sensitive to excess porewater pressures - a property that is inherently variable in real geotechnical problems. Underestimation of r_u can lead to underprediction of observed lateral spreading displacements, while higher values of r_u may cause large displacements, particularly near the soil surface. The sensitivity analysis does also exhibit a behavior that is intuitive – lower r_u values arrest lateral spreading displacements. However, permanent displacements from r_u values less than unity may still occur, demonstrating a need to evaluate excess porewater pressure generation even when “full liquefaction” (i.e., r_u = 1) is not realized.

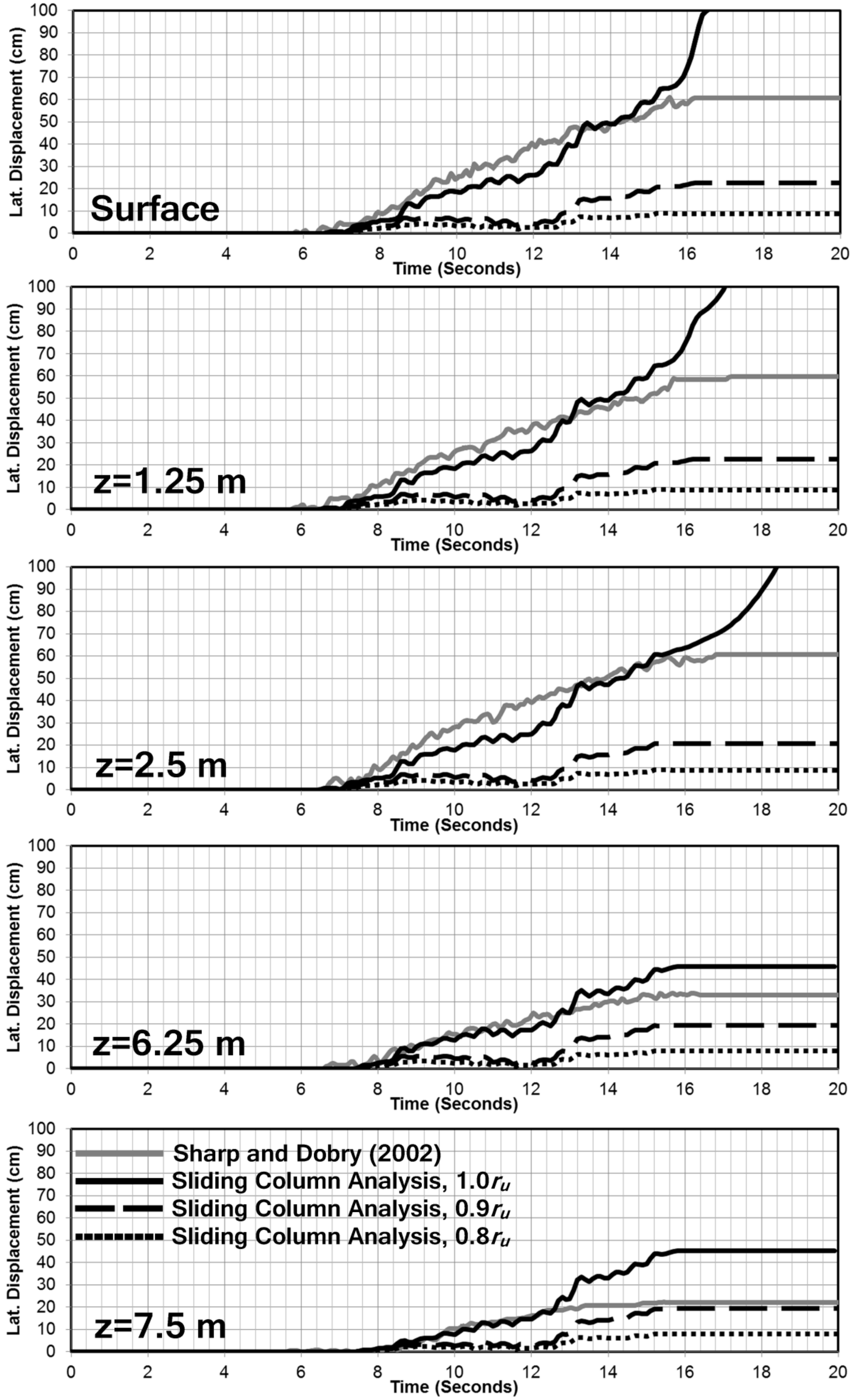
Surface
z=1.25 m
z=2.5 m
z=6.25 m
z=7.5 m
Lat. Displacement (cm)
Time (Seconds)
Sharp and Dobry (2002)
Sliding Column Analysis, 1.0r_u
Sliding Column Analysis, 0.9r_u
Sliding Column Analysis, 0.8r_u

Figure 8. Effect of excess porewater pressure ratio, r_u, on lateral spreading displacements.

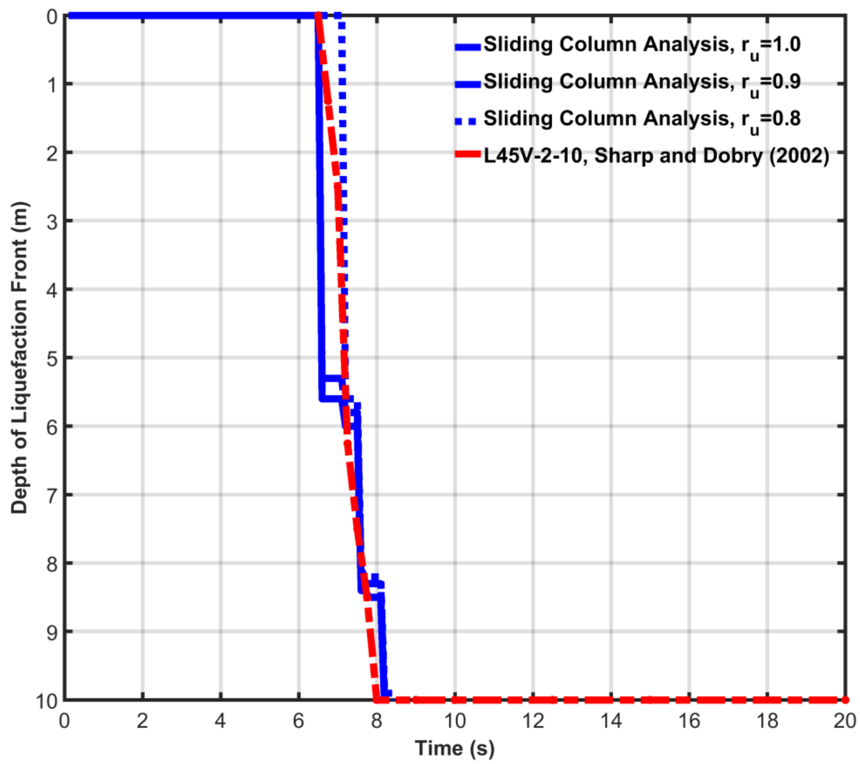

Figure 9. Effect of excess porewater pressure ratio, r_u, on depth of liquefaction front.

Implications of Cohesion and Cementation

The effects of true cohesion, primarily stemming from cementation, can significantly influence the arrest of liquefaction (Clough et al. 1989, Mitchell et al. 1995). Light cementation is common in naturally deposited sands or sands improved with admixtures (Huang and Airey 1998). The effects of cementation are evaluated from the results of LV45-2-10, applied as 5, 10 and 20 kPa of cohesion. The results, shown in Figure 10, demonstrate a significant arrest of displacements, particularly at the surface, which exhibited large modeled displacements when cohesionless. The arrest of displacements are amplified when cohesion is increased further, demonstrated by a reduction of surface displacement from 23 cm to 5 cm for cohesion values of 5 and 20 kPa, respectively. Cohesion effects are also observed in the lateral earth pressure and shear strain profiles (Figure 11), where cohesion stabilizes the failing surface layer and mutes the shear strains at greater depths. Increasing cohesion, as expected, decreases the earth pressures, particularly near the surface, both before and after shaking. The effects of true cohesion stemming from natural or artificial cementation intuitively demonstrate improved performance during seismic excitation and porewater pressure buildup owing to increased internal shear strength and resistance to failure, particularly at shallow depths. From a practical perspective, artificial and especially natural cementation is an inherently spatially variable, suggesting that judgment must be used if cementation is considered as a means of lateral spreading mitigation. However, the benefits of even light cementation are significant.

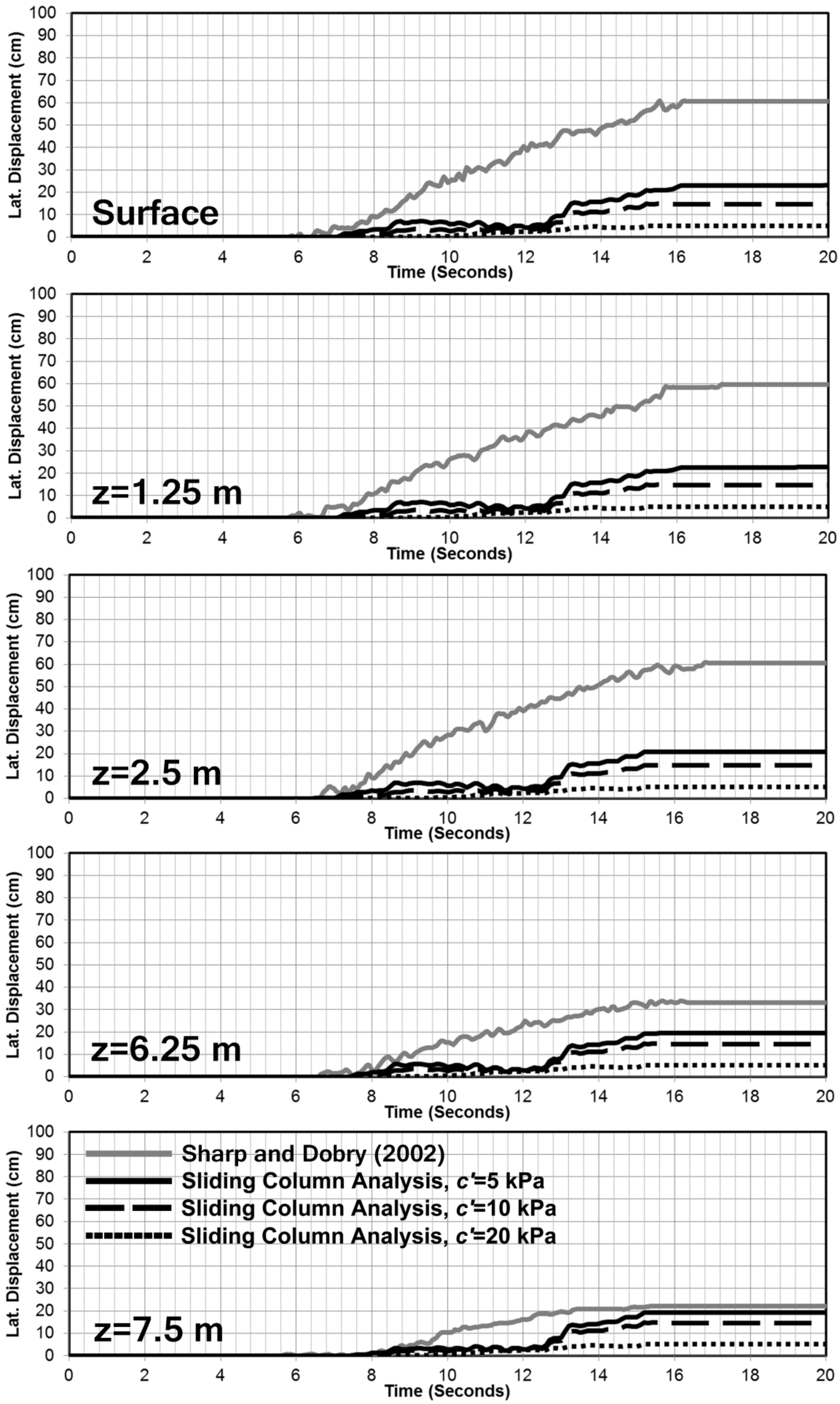
Surface
z=1.25 m
z=2.5 m
z=6.25 m
z=7.5 m
Lat. Displacement (cm)
Time (Seconds)
Sharp and Dobry (2002)
Sliding Column Analysis, c'=5 kPa
Sliding Column Analysis, c'=10 kPa
Sliding Column Analysis, c'=20 kPa

Figure 10. Effect of cohesion on lateral spreading displacements.

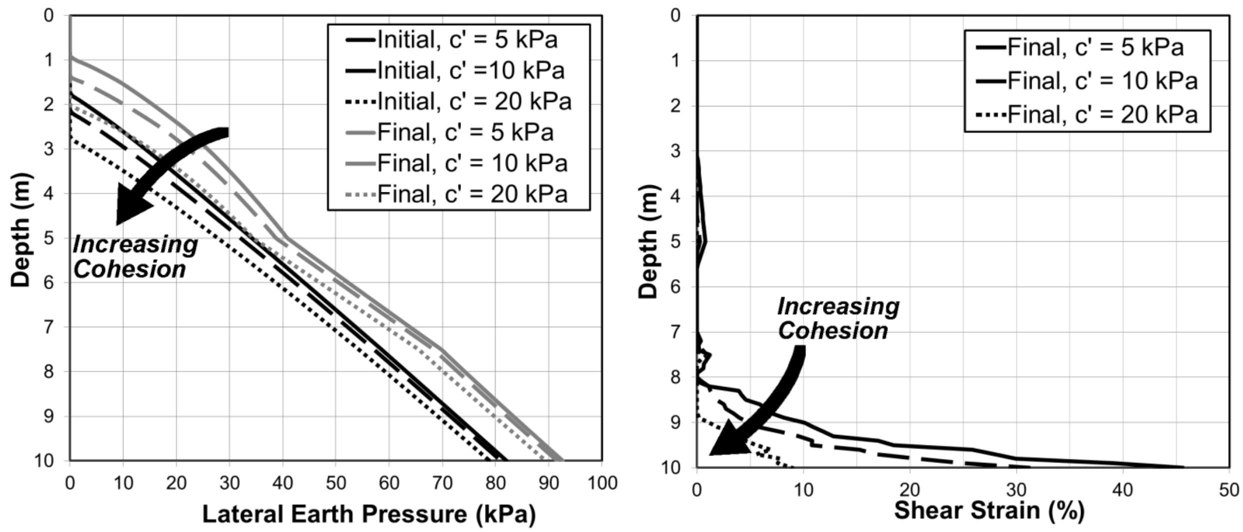

Figure 11. Effect of cohesion on lateral earth pressures and shear strains.

Application to Layered Soils

To illustrate application towards layered soils, a soil profile consisting of a two meter thick liquefiable seam is considered. The top seven meters consist of lightly cemented sand (γ_{sat}=20kN/m^3, ϕ'=35°, c'=10kPa), underlain by loose, liquefiable sand (γ_{sat}=19.4kN/m^3, ϕ'=35°, c'=0kPa) and a layer of dense, heavily cemented silty sand (γ_{sat}=21kN/m^3, ϕ'=35°, c'=50kPa), all inclined at a 5° angle – see Figure 12. For the given profile, the same excess porewater pressure regime and input motion used in previous sections was considered. At the end of the twenty seconds of shaking, there is a demonstrated concentration of shear strains (up to 12%) within the cohesionless, liquefiable layer (Figure 12). This results in permanent lateral displacements of approximately 7 cm constrained to the seam of liquefying soil. This example demonstrates the importance of characterizing problematic seams of liquefiable soil within profiles of relatively competent material. When the stratigraphy and the properties of underlying soils are well-characterized, the proposed model may capture the localized failure and subsequent displacement of weak, liquefiable seams.

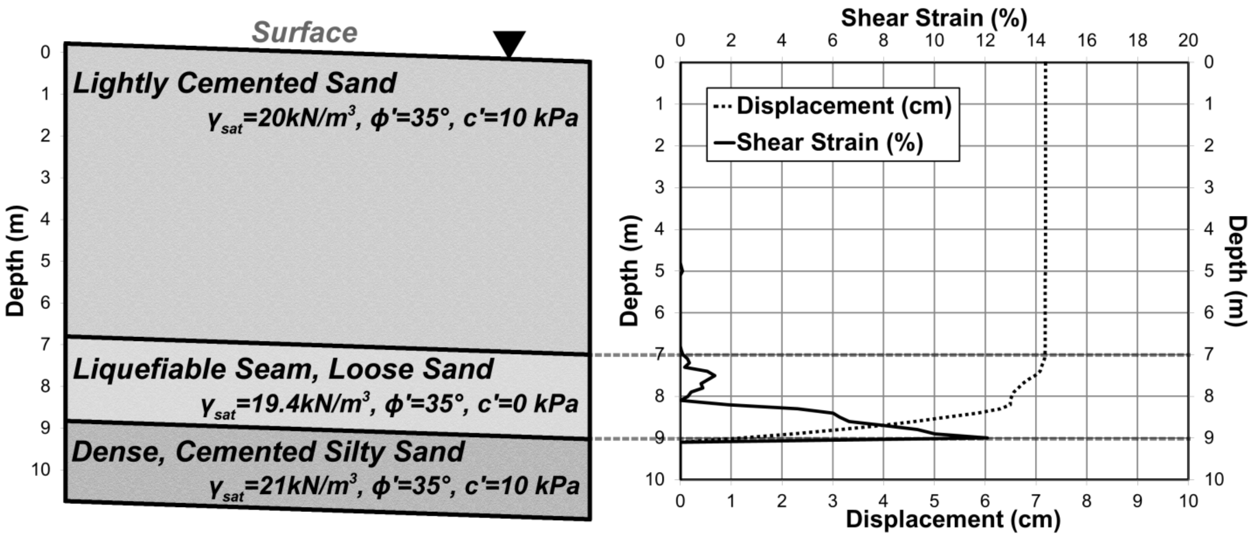

Figure 12. Left: Example layered soil profile with a subsurface weak seam of sand. Right: Modeled shear strains and displacements for given profile.

Free Face Effects

To exhibit the effects of a free face, an example consisting of a partially saturated, organic crustal slope that has a height of 5 meters, a width of 30 meters, and a steep 45° face is placed on a gently sloping layer of saturated sand (subsurface slope of β) overlying a competent, non-liquefiable basal layer (Figure 13). The crustal layer and saturated sand layer have total unit weights of 10.2 kN/m^3 and 19.4 kN/m^3, respectively. The crustal layer has a cohesion of 10 kPa and an internal angle of friction of 30°. The saturated sand layer beneath the crustal layer is cohesionless and has an internal angle of friction of 35°. A sensitivity study was performed on several subsurface slopes (β=0°, 1°, 3° and 5°) for the same seismic inputs from LV45-2-10 (Sharp and Dobry 2002). The cyclic behavior of the excess porewater pressures within the soil profile is similar to that from that of Sharp and Dobry (2002), but the maximum magnitudes were changed to vary from zero to 90 kPa at the basal layer (Figure 13).

The results demonstrate that lateral spreading displacements decrease with diminishing subsurface slopes, but still demonstrate displacements on horizontal liquefying sand layers (Figure 14). When transitioning from β=0° to β=5°, the maximum lateral displacements increase from approximately 4 cm to approximately 46 cm. Notably, the difference between driving and resisting at-rest forces due to uneven overburden along the width of a sliding block results in increased movement during liquefaction, particularly with seismic motions. Although the displacement for horizontal ground is limited in this example, very gentle, sloping liquefiable layers of 1° and 3° result in 9 and 22 cm of displacement (Figure 14), respectively, which may compromise buried utilities and sewers.

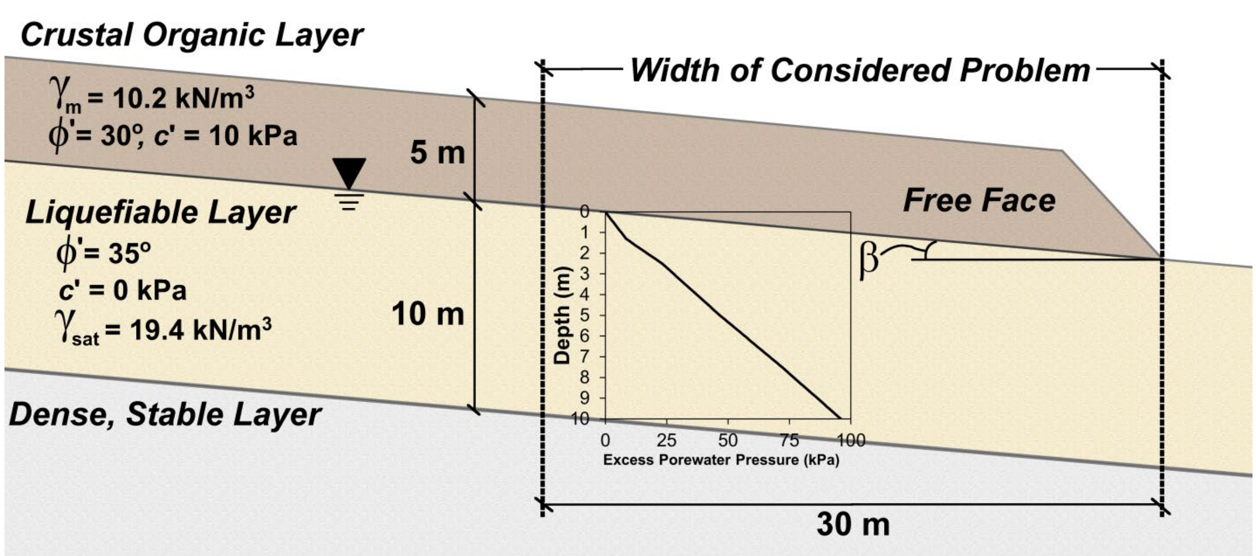

Figure 13. Example profile analyzed in the free face lateral spread scenario.

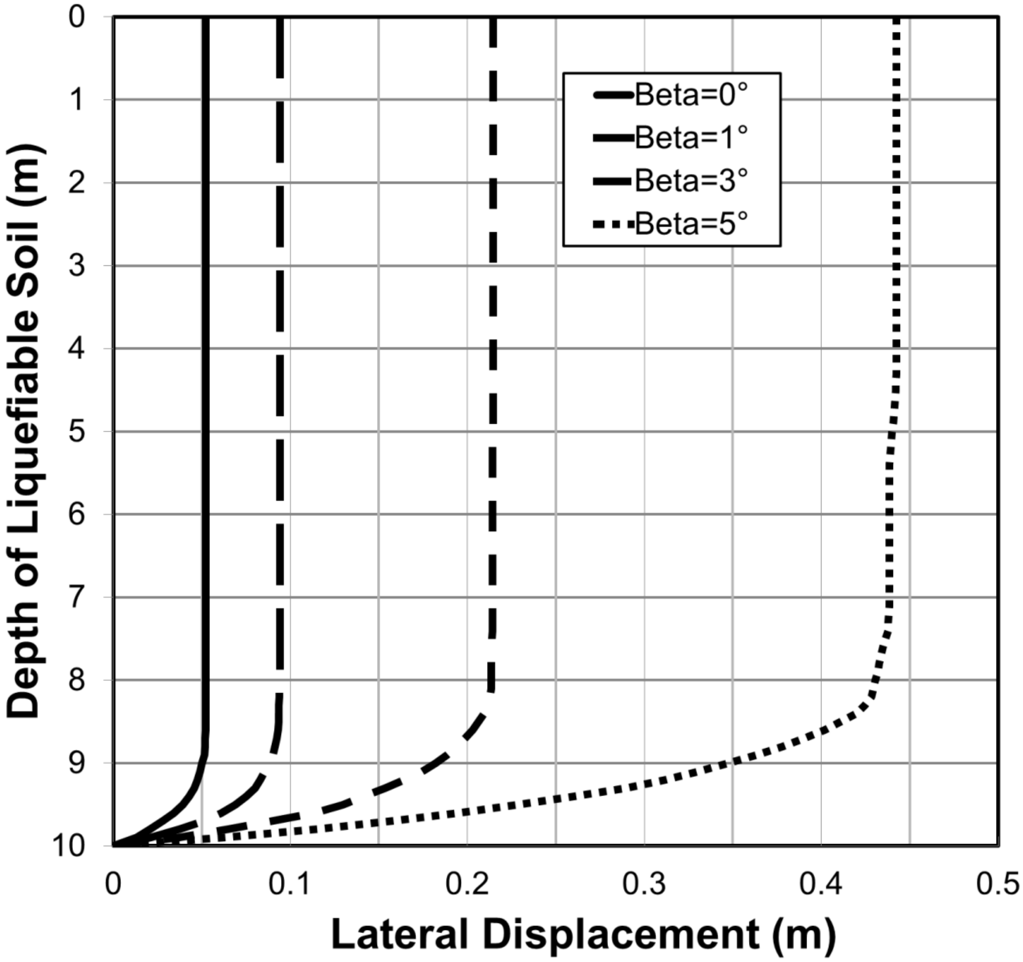

Figure 14. Effect of liquefiable layer inclination on free face movements for discrete, coherent sliding mass.

CONCLUSIONS

Liquefaction-induced lateral spreading behavior was investigated using a Newmark-type limit equilibrium framework comprised of a column of sliding blocks subject to changing yield accelerations and seismic accelerations. A contribution of this work is that it analyzes lateral spreading within a deterministic, limit equilibrium-based slope stability framework instead of traditional statistical or experimental approaches. Notably, the primary focus of the article was presenting the application of the modified Newmark framework for evaluating lateral spread displacements. In its current form, this tool presents itself as a useful supplement, or check, for determining lateral spreading displacements in comparison to more complex site-specific analyses that necessitate use of numerical methods. In the future, this framework can be expanded to account for different failure kinematics, incorporate more complex soil constitutive or hydraulic properties, account for site response analyses, or even incorporate data from numerical models. Because the methodology considers physical data, it may provide more reliable results than empirical-based lateral spreading displacement procedures when a subsurface is well-defined. The simplicity of the framework in its current form makes it less suited for site-specific analyses, but transferrable towards regional assessments of lateral spreading displacements. There are limited deterministic methods for regional evaluation of lateral spreading displacements that can incorporate subsurface data – this framework will enable such assessments. Such an analysis is useful for planning purposes as well as for rapid analysis to support post-earthquake reconnaissance.

The presented sliding column analysis captures the general behavior of lateral spreading in the free field when compared to well-instrumented centrifuge testing. Some disagreement occurs due to instability of Newmark sliding blocks at the surface, particularly for very low yield accelerations. Nonetheless, the sliding column analysis can capture shear strains and displacements within a given soil profile during lateral spreading and predicts larger earth pressures at notable liquefaction fronts. The presented analysis is sensitive to the effective stress of the soil column, predicting significant instability for excess porewater pressure coefficients near unity, with arrested, but still significant displacements, for lower porewater pressures. The effects of soil cementation are pronounced for arresting lateral spread displacements, and soil cementation effects are more pronounced at the ground surface. The proposed model can incorporate layers of soil with a well-characterized subsurface, isolating localized seams of unstable material. The effects of free face on lateral spreading displacements are more pronounced when the liquefying later inclination increases. However, lateral spreading still occurs for a horizontal liquefying layer as the inertial loading and difference in surrounding at-rest earth forces destabilize the block.

The sliding column analysis, although applicable with basic geotechnical properties, has several constraints and uncertainties that deserve further refinement. In particular, Newmark-type analyses for evaluating displacements of rigid block using a limit equilibrium framework may diverge and overpredict displacements when the yield acceleration is exceeded significantly (Kramer and Lindwall 2004). Incorporation of material properties, such as dilation and the viscosity of liquefied soil, may mitigate aforementioned weaknesses of Newmark-type analyses – leading to better lateral spreading displacement and earth pressure predictions. Furthermore, seismic earth pressures in saturated soils are dependent on more complex soil behavior, which is difficult to capture within a limit equilibrium-based model; namely, the omission of viscous soil behavior and incorporation of seismic boundary effects. Another potential weakness includes the need to input an excess porewater pressure-time series. The excess porewater pressure-time series can be developed from one-dimensional or two-dimensional site response analyses for a given earthquake motion and soil profile with appropriate dynamic soil properties (and an assumption for how strain is related to pore water pressure generation). In addition, the excess porewater pressure-time series can be developed using more complete numerical modeling techniques with soil constitutive models. However, using the aforementioned methods may negate some of the benefits of the modified Newmark method; mainly, the simplicity of the method. Accordingly, for future application, we recommend using a simplified porewater pressure estimation method (e.g., Seed et al. 1977) to develop reasonable excess porewater pressure-time series.

Notwithstanding potential weaknesses of the Newmark-type analysis, the presented analysis is appropriate for simple modeling of lateral spreading displacements. The model can be used to investigate the effect of varying soil density, frictional strength, and excess porewater pressures with depth, which is important for integrating geotechnical site investigation data (e.g. CPT, SPT). Furthermore, the effects of a crustal surface layer with two-dimensional topography can be implemented, providing a means of describing the notable lateral spread occurrence at the confluence of gentle slopes and bodies of water. The simplified analysis also demonstrates promise for applicability to a larger scale, particularly implementation through use of combined digital elevation models and site investigation databases, providing an opportunity to create a deterministic hazard mapping procedure as had been done using statistical methods (e.g., Youd and Perkins 1987, Bardet et al. 2002, Rosinski et al. 2004, Olsen et al. 2007, Gillins 2012). Finally, the model can be further enhanced to handle more complex problems by (1) evaluating alternative failure mechanisms, (2) incorporating seismic boundary forces more robustly,

(3) incorporating models relating coupled or decoupled seismic accelerations throughout the soil column, and (4) implementing models relating the buildup of excess porewater pressures throughout the soil profile.

References

1. Abdoun, T., Dobry, R., O'Rourke, T. D., & Goh, S. H. (2003). Pile response to lateral spreads: centrifuge modeling. *Journal of Geotechnical and Geoenvironmental Engineering*, *129*(10), 869-878.
2. Abdoun, Tarek, and Ricardo Dobry. "Evaluation of pile foundation response to lateral spreading." *Soil Dynamics and Earthquake Engineering* 22.9 (2002): 1051-1058.
3. Arulmoli, K., Muraleetharan, K.K., Hossain, M.M., and Fruth, L.S. 1992. VELACS, verification of liquefaction analyses by centrifuge studies — laboratory testing program — soil data report. Technical report prepared for the National Science Foundation by The Earth Technology Corporation, Irvine, Calif. Available from http://geoinfo.usc.edu/gees/velacs/
4. Bardet, J. P., Tobita, T., Mace, N., and Hu, J., 2002. Regional modeling of liquefaction-induced ground deformation, *Earthquake Spectra* **18**(1), 19-46.
5. Bartlett, S. F., & Youd, T. L. (1995). Empirical prediction of liquefaction-induced lateral spread. *Journal of Geotechnical Engineering*, *121*(4), 316-329.

6. Biondi, G., Cascone, E., Maugeri, M., & Motta, E. (2000). Seismic response of saturated cohesionless slopes. *Soil Dynamics and Earthquake Engineering*, *20*(1), 209-215.
7. Boulanger, R. W., Meyers, M. W., Mejia, L. H., & Idriss, I. M. (1998). Behavior of a fine-grained soil during the Loma Prieta earthquake. *Canadian Geotechnical Journal*, *35*(1), 146-158.
8. Boulanger, R., Mejia, L., and Idriss, I. (1997). "Liquefaction at Moss Landing during Loma Prieta Earthquake." *J. Geotech. Geoenviron. Eng*., 10.1061/(ASCE)1090-0241(1997)123:5(453), 453-467.
9. Brandenberg, S. J., Boulanger, R. W., Kutter, B. L., & Chang, D. (2007). Liquefaction-induced softening of load transfer between pile groups and laterally spreading crusts. *Journal of geotechnical and geoenvironmental engineering*, *133*(1), 91-103.
10. Brandenberg, S. J., Boulanger, R. W., Kutter, B. L., & Chang, D. (2005). Behavior of pile foundations in laterally spreading ground during centrifuge tests. *Journal of Geotechnical and Geoenvironmental Engineering*, *131*(11), 1378-1391.
11. Clough, G. W., Iwabuchi, J., Rad, N. S., & Kuppusamy, T. (1989). Influence of cementation on liquefaction of sands. *Journal of Geotechnical Engineering*, *115*(8), 1102-1117.
12. Geraili, R., & Sitar, N. (2013). Seismic Earth Pressures on Retaining Structures in Cohesionless Soils.

13. Gillins, D. and Bartlett, S. (2013). "Multilinear Regression Equations for Predicting Lateral Spread Displacement from Soil Type and Cone Penetration Test Data." *J. Geotech. Geoenviron. Eng.*, 10.1061/(ASCE)GT.1943-5606.0001051, 04013047.

14. Gillins, D.T., 2012. "Mapping the probability and uncertainty of liquefaction-induced ground failure." *PhD Dissertation, University of Utah.*

15. Huang, J. T., & Airey, D. W. (1998). Properties of artificially cemented carbonate sand. *Journal of Geotechnical and Geoenvironmental Engineering*, *124*(6), 492-499.

16. Javadi, A. A., Rezania, M., & Nezhad, M. M. (2006). Evaluation of liquefaction induced lateral displacements using genetic programming.*Computers and Geotechnics*, *33*(4), 222-233.

17. Jibson, R. W. (2011). Methods for assessing the stability of slopes during earthquakes—A retrospective. *Engineering Geology*, *122*(1), 43-50.

18. Kramer, S. and Lindwall, N. (2004). "Dimensionality and Directionality Effects in Newmark Sliding Block Analyses." *J. Geotech. Geoenviron. Eng.*, 10.1061/(ASCE)1090-0241(2004)130:3(303), 303-315.

19. Kramer, S. and Smith, M. (1997). "Modified Newmark Model for Seismic Displacements of Compliant Slopes." *J. Geotech. Geoenviron. Eng.*, 10.1061/(ASCE)1090-0241(1997)123:7(635), 635-644.

20. Kramer, S. L., & Smith, M. W. (1997). Modified Newmark model for seismic displacements of compliant slopes. *Journal of Geotechnical and Geoenvironmental Engineering*, *123*(7), 635-644.

21. Matasovic, N., & Kavazanjian Jr, E. (1997). *Newmark deformation analysis with degrading yield acceleration* (No. Volume 2).
22. Mitchell, J. K., Christopher, D., Baxter, P., and Munson, T. C. 1995. “Performance of improved ground during earthquakes.” Geotech. Spec. Publ., 49, 1–36.
23. Newmark, N. M. (1965). “Effects of earthquakes on dams and embankments.” Geotechnique, 15(2), 139–160.
24. Olsen, M. J., Bartlett, S. F., and Solomon, B. J., 2007. Lateral spread hazard mapping of the Northern Salt Lake Valley, Utah for a M7.0 scenario earthquake, *Earthquake Spectra* **23**(1), 95-113.
25. Olson, S. and Johnson, C. (2008). "Analyzing Liquefaction-Induced Lateral Spreads Using Strength Ratios." *J. Geotech. Geoenviron. Eng*., 10.1061/(ASCE)1090-0241(2008)134:8(1035), 1035-1049.
26. Rathje, E. and Bray, J. (2000). "Nonlinear Coupled Seismic Sliding Analysis of Earth Structures." *J. Geotech. Geoenviron. Eng*., 10.1061/(ASCE)1090-0241(2000)126:11(1002), 1002-1014.
27. Rauch, A. F., and Martin, J. R. (2000). “EPOLLS model for predicting average displacements on lateral spreads.” *J. Geotech. Geoenviron. Eng.* 126(4), 360-371.
28. Rosinski, A., Knudsen, K. L., Wu, J., Seed, R. B., and Real, C. R., 2004. Development of regional liquefaction-induced deformation hazard maps, in *GeoTrans 2004, Geotechnical Engineering for Transportation Projects (GSP No.*

126), M. K. Yegian and E. Kavazanjian (editors), ASCE, Los Angeles, CA, pp. 797-806.

29. Taboada-Urtuzuástegui, V. and Dobry, R. (1998). "Centrifuge Modeling of Earthquake-Induced Lateral Spreading in Sand*." J. Geotech. Geoenviron. Eng*., 10.1061/(ASCE)1090-0241(1998)124:12(1195), 1195-1206.
30. Towhata, I., Sasaki, Y., Tokida, K., Matsumoto, H., Tamari, Y., & Yamada, K. (1992). Prediction of permanent displacement of liquefied ground by means of minimum energy principle. *Soils and Foundations*, *32*(3), 97-116.
31. Vucetic, M. (1994). Cyclic threshold shear strains in soils, *Journal of Geotechnical Engineering* 120(12), 2208-2228.
32. Wartman, J., Bray, J. D., & Seed, R. B. (2003). Inclined plane studies of the Newmark sliding block procedure. *Journal of Geotechnical and Geoenvironmental Engineering*, *129*(8), 673-684.
33. Whitman, R. V., & Liao, S. (1985). *Seismic design of gravity retaining walls*. Massachusetts Inst of Tech Cambridge Dept of Civil Engineering.
34. Youd, T. L., & Perkins, D. M. (1987). Mapping of liquefaction severity index. *Journal of Geotechnical Engineering*, *113*(11), 1374-1392.
35. Youd, T. L., Hansen, C. M., & Bartlett, S. F. (2002). Revised multilinear regression equations for prediction of lateral spread displacement. *Journal of Geotechnical and Geoenvironmental Engineering*, *128*(12), 1007-1017.
36. Zhang, G., Robertson, P. K., and Brachman, R. W. (2004). “Estimating liquefaction-induced lateral displacements using the standard penetration test or cone penetration test.” *J. Geotech. Geoenviron. Eng.* 130(8), 861-871.